Contents lists available at ScienceDirect

Applied Catalysis B: Environmental

Ordered macroporous Bi_2O_3/TiO_2 film coated on a rotating disk with enhanced photocatalytic activity under visible irradiation

Yuning Huo [a,*], Xiaofang Chen [a], Jia Zhang [a], Gaifang Pan [a], Jinping Jia [b,**], Hexing Li [a,*]

[a] The Education Ministry Key Lab of Resource Chemistry and Shanghai Key Laboratory of Rare Earth Functional Materials, Shanghai Normal University, Shanghai 200234, PR China
[b] School of Environmental Science and Engineering, Shanghai Jiao Tong University, Shanghai 200240, PR China

ARTICLE INFO

ABSTRACT

Ordered macroporous Bi_2O_3/TiO_2 film coated on a rotating disk was prepared by sol–gel method in the presence of polystyrene (PS) microspheres as a template, which showed spectral response in visible region via Bi_2O_3 photosensitizing effect and low photoelectron-hole recombination by forming Bi_2O_3-TiO_2 heterojunctions. Meanwhile, the ordered macropores in the Bi_2O_3/TiO_2 film promoted light-harvesting via multiple reflections and also facilitated reactant adsorption owing to the diminished diffusion limit and enhanced surface hydrophilicity. More importantly, the rotating disk could effectively reduce the light shielding on the Bi_2O_3/TiO_2 film photocatalyst, especially in the color solution. As a result, the as-prepared Bi_2O_3/TiO_2 film exhibited high activity in aqueous visible-light-driven photocatalytic degradation of single and mixed dyes or reduction of Cr^{6+} to Cr^{3+}.

© 2013 Elsevier B.V. All rights reserved.

1. Introduction

Photocatalysis has been considered to be effective in mineralizing organic contaminants in wastewater using solar lights [1,2]. TiO_2 photocatalyst is frequently employed owing to its high activity, cheapness, non-toxicity and stability, but it cannot be activated by visible lights due to the big energy gap [3,4]. Both composition modification and nanoscale structure engineering are necessary to achieve high activity under solar lights irradiation [5,6]. Up to now, a great number of TiO_2 modified with metal or metal ions [7,8], nonmental [9], semiconductors [10] and dyes [11] have been designed to achieve visible photocatalysts. The Bi_2O_3/TiO_2 has been widely recognized as an active visible photocatalyst via the photosensitizing effect of Bi_2O_3 [12,13] and the reduced photoelectron-hole recombination rate by forming Bi_2O_3-TiO_2 heterojunctions [14,15]. Meanwhile, it has also reported that photocatalyst morphology and pore structure as well as surface chemistry greatly influence light harvest, photoelectron-hole recombination rate, diffusion

and adsorption of reactant molecules [16–19]. Obviously, the three-dimensionally ordered macropores (3DOM) is favorable for photocatalytic activity owing to the enhanced light harvest via multiple reflections and decreased diffusion limit [20–22].

To date, most composition modification and structural engineering are focused on powder photocatalysts due the easy preparation and operation. However, the practical applications of powder photocatalysts are limited due to their difficult separation and reuse. Meanwhile, during liquid phase photocatalysis, the powder photocatalysts usually display poor light absorbance due to the shielding effect on light irradiation from solution, especially from the color solution containing dyes or heavy metallic ions. Recently, we developed a photocatalytic reactor containing a rotating disk coated with photocatalyst [23]. The disk was partially immersed in solution which could effectively avoid light shielding from color solution by rotating the disk (see Fig. 1). Up to now, only the pure TiO_2 film has been coated on the disk, which limits the practical application under solar lights irradiation. It is still a challenging task to design doped TiO_2 film with controllable structure. Herein, we reported a facile approach to coat ordered macroporous Bi_2O_3/TiO_2 film onto the glass sheets by sol–gel route in the presence of polystyrene (PS) microspheres as the hard template. This Bi_2O_3/TiO_2 film photocatalyst coated on the rotating disk exhibited high activity during liquid phase photocatalytic degradation of

* Corresponding authors. Tel.: +86 21 64322642; fax: +86 21 64322272.
** Corresponding author. Tel.: +86 21 54742817; fax: +86 21 54742817.
E-mail addresses: Huoyuning@shnu.edu.cn (Y. Huo), Jpjia@sjtu.edu.cn (J. Jia), HeXing-Li@shnu.edu.cn (H. Li).
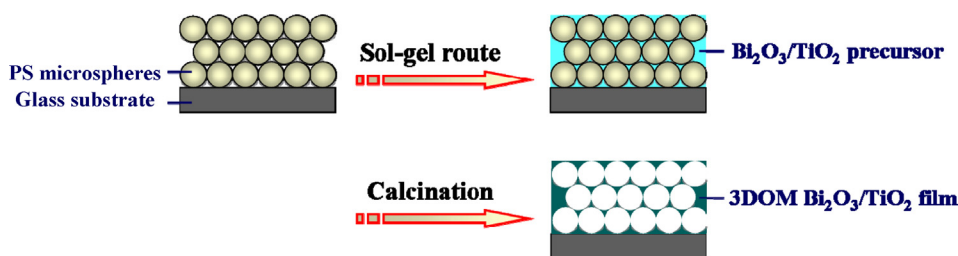
Scheme 1. Illustration of the process for preparing 3DOM Bi_2O_3/TiO_2 film coated onto a glass substrate *via* sol–gel route by using PS microspheres as the template.

methylene blue (MB) under visible light irradiation. Meanwhile, it was also applied for degradation of mixed dyes and reduction of Cr^{6+} in wastewater.

2. Experimental

2.1. Sample preparation

The Bi_2O_3/TiO_2 film coated onto a glass substrate was prepared by sol–gel route in the presence of PS microspheres as the template (see Scheme 1). Firstly, PS microspheres were prepared by emulsifier-free batch emulsion polymerization [24]. Then, a glass substrate (2.5 cm × 2.0 cm) was treated with 1.0 mol/L NaOH solution for 1 h, followed by ultrasonically cleaning with acetone and washing with ethanol and water for 3 times, respectively. After being dried in air, the glass substrate was immersed vertically in the aqueous suspension containing 0.20 wt% PS microspheres and kept at 60 °C for 24 h to achieve the colloidal crystal film on the glass surface, followed by heating at 85 °C for 30 min to enhance the interaction. Subsequently, the Bi_2O_3/TiO_2 precursor was prepared by sol–gel method described as follows. 1.0 mL $TiCl_4$ was added dropwise into 20 mL ethanol solution and stirred at 25 °C for 5 min. Then, desired amount of $Bi(NO_3)_3 \cdot 5H_2O$ was added and stirred for 30 min, followed by adding 3.0 mL tetrabutyl titanate and stirring for 2 h. The as-received Bi_2O_3/TiO_2 precursor gel was then dropped onto the PS colloidal crystal film coating on the glass substrate with 15° inclination angle, followed by evaporating solvent, drying at ambient temperature, and finally calcining at 500 °C for 4 h to remove the template, leading to the 3DOM Bi_2O_3/TiO_2 film. The film weight was determined as 3.6 ± 0.9 mg. The Bi content was adjusted by changing $Bi(NO_3)_3 \cdot 5H_2O$ amount in the mother solution and denoted as $X\%$ Bi_2O_3/TiO_2, where $X\%$ refers to Bi/Ti molar ratio. Meanwhile, the thickness of Bi_2O_3/TiO_2 film was adjusted by changing the amount of PS microspheres coated on the glass surface. For comparison, 1.0% $Bi_2O_3/TiO_2(N)$ film without 3DOM structure was also prepared by the same way in the absence of PS template. Its film weight was similar to that of 1.0% Bi_2O_3/TiO_2 film.

2.2. Characterization

The photocatalyst structure was determined by X-ray diffraction patterns recorded on Rigaku Dmax-3C with Cu Kα radiation. Surface morphologies were observed by scanning electron microscopy (FESEM, HITACHI S-4800) and transmission electronic microscopy (TEM, JEM-2010). X-ray photoelectron spectroscopy (XPS, Versa Probe PHI 5000) was employed to determine surface electronic states. All the binding energy values were calibrated by using $C_{1S} = 284.6$ eV as a reference. N_2 adsorption–desorption isotherms were measured on a Quantachrome NOVA 4000e. The specific surface area (S_{BET}) and pore size distribution were obtained by applying multiple-point Brunauer–Emmett–Teller (BET) and Barrett–Joyner–Halenda (BJH) models on the adsorption branches. The optical properties were determined by UV–vis diffuse reflectance spectrum (DRS, Cary 500, Varian) and photoluminescence spectrum (PLS, Varian Cary-Eclipse 500). The contact angle of water droplet on the film was measured by the sessile drop method at 20 °C on a JC2000D contact angle analyzer. All measurements were performed at five spots on the surfaces. Photocurrent measurement was carried out on a CHI electrochemical analyzer (CHI 660D) in a standard three-electrode configuration with 0.2 mol/L Na_2SO_4 electrolyte. The Bi_2O_3/TiO_2 films coated on the substrate of ITO conductive glass was used as the photoanode (surface area = 4.0 cm^2), while a Pt foil and a saturated calomel electrode (SCE) were used as the counter electrode and the reference electrode, respectively. A 300 W Xe lamp was used as the light source with the distance of 10 cm to the surface of photoanode. The lights with wavelength less than 400 nm were removed by a glass filter (JB-400).

2.3. Adsorption test

Three glass sheets coated with photocatalysts were immerged into 5.0 mL 10 mg/L MB solution at 30 °C. At given time intervals, the initial concentration of MB (C_0) and MB concentration during the adsorption process (C) were measured on a UV–vis spectrophotometer (UV-7502PC, XinMao Instrument Co. Ltd, Shanghai) to calculate the adsorption rate, according to the light absorbance at the characteristic peak of 664 nm. In addition, the instant adsorption capability of different samples was investigated. The film coated on one glass sheet (2.0 cm × 2.5 cm) was immerged into 5.0 mL 10 mg/L MB solution at 30 °C and kept for 1 s. After being dried, the light absorbance of MB adsorbed on the film was measured on a UV–vis spectrophotometer.

2.4. Activity test

The self-designed reactor containing a poly (methylmethacrylate) (PMMA) disk (75 mm in diameter) with
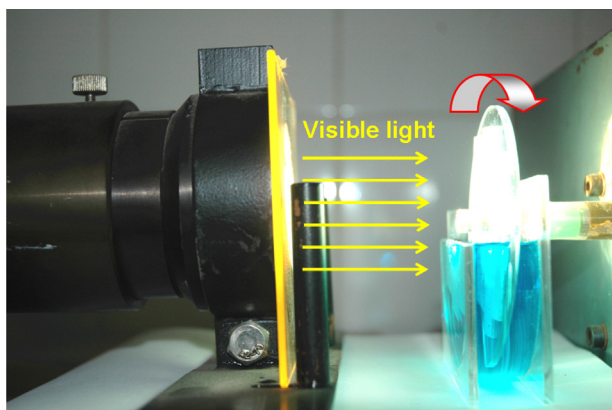
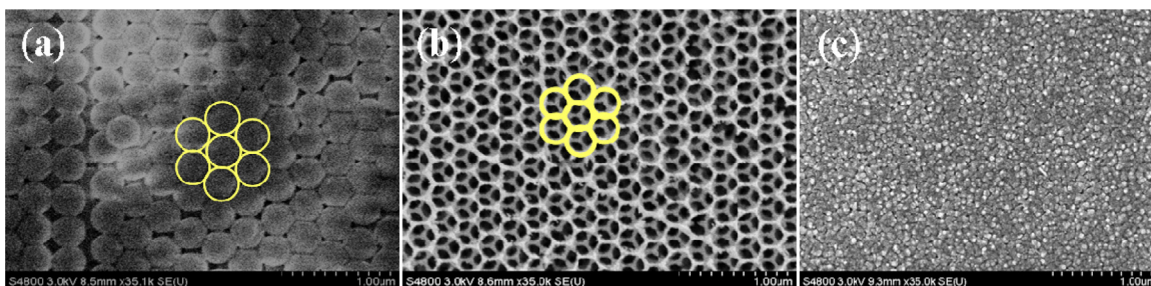**Fig. 1.** Photocatalytic reactor containing a rotating disk coated with Bi_2O_3/TiO_2 film photocatalyst.

Fig. 2. FESEM images of (a) PS colloidal crystal template, (b) 1.0% Bi_2O_3/TiO_2 film and (c) 1.0% $Bi_2O_3/TiO_2(N)$ film on glass substrate.

Table 1
Structural parameter of different samples.

Sample	TiO_2	0.2%Bi_2O_3/TiO_2	1.0%Bi_2O_3/TiO_2	1.5%Bi_2O_3/TiO_2	2.0%Bi_2O_3/TiO_2	1.0%$Bi_2O_3/TiO_2(N)$
S_{BET} (m^2/g)	21	25	43	33	28	31

photocatalyst films was used to evaluate the photocatalytic activity (see Fig. 1). In a typical run of reactions, 6 glass sheets coated with photocatalyst were uniformly localized on the disk and immerged into 55 mL 10 mg/L MB solution with 57% surface area exposed to the air. Before each run of photocatalysis, the disk was rotated at the speed of 90 rpm for 30 min in the dark until reaching the adsorption–desorption equilibrium. Then, the photocatalysis process was initiated by irradiation with a 500 W Xe lamp at a distance of 4.0 cm. To make sure that the photocatalytic reaction was really driven by visible-light, all the UV lights with the wavelength less than 420 nm were removed by a glass filter (JB-420). At given time intervals, the concentration of MB was determined by measuring light absorbance using UV–vis spectrophotometer. Preliminary tests revealed that only less than 5.0% MB was removed in the absence of either light irradiation or photocatalyst, and thus could be neglected in comparison with the MB degradation yield *via* photocatalysis process (Table 1). The reproducibility of the results was checked by repeating the experiments at least three times and was found to be within acceptable limits ($\pm$5%).

The photodegradation tests of aqueous solutions mixed with different substrates including MB, rhodamine B (RhB), methyl orange (MO) and Cr^{6+} were carried out under the same reaction conditions as mentioned above. The concentration of each substrate was 10 mg/L in the mixture solution. Liquid chromatography-mass spectrometry (HPLC-MS, Angilent 1200) was used to detect the dyeing compounds. The concentration of Cr^{6+} left in aqueous solution was analyzed by UV spectrophotometer at its characteristic wavelength (λ = 369 nm).

3. Results and discussion

3.1. Structural characteristics

The FESEM images in Fig. 2 revealed that the PS microspheres with average diameter of 300 nm were uniformly dispersed onto the glass substrate. The 1.0% Bi_2O_3/TiO_2 film displayed three-dimensionally ordered macropores (3DOM) with average pore diameter around 270 nm and pore-wall thickness around 35 nm. However, 1.0% $Bi_2O_3/TiO_2(N)$ film prepared without PS microspheres only presented the particle distribution without macropores. These results demonstrated that the macropores in the Bi_2O_3/TiO_2 film were templated by PS microspheres. The slight decrease in pore diameter could be attributed to the shrinkage during calcinations to remove PS microsphere template. The TEM image in Fig. S1 also presented the obvious 3DOM structure in the Bi_2O_3/TiO_2 film.

The XPS spectra (Fig. 3) demonstrated that all Bi species in 1.0% Bi_2O_3/TiO_2 film were presented in Bi_2O_3 phase, corresponding to the binding energies of 158.9 and 164.2 eV in $Bi_{4f7/2}$ and $Bi_{4f5/2}$ levels, respectively. No significant change in the XPS spectra of either Ti_{2p} or O_{1s} was observed in comparison with the pure TiO_2 [12,13], suggesting that the Bi_2O_3 was present mainly in separated phase rather than incorporated into the TiO_2 lattice, which could be easily understood by considering much bigger size of Bi atom (103 pm) than that of Ti atom (61 pm) [25].

As shown in Fig. 4, the XRD patterns revealed all the Bi_2O_3/TiO_2 films with different Bi_2O_3 contents and the 1.0% $Bi_2O_3/TiO_2(N)$
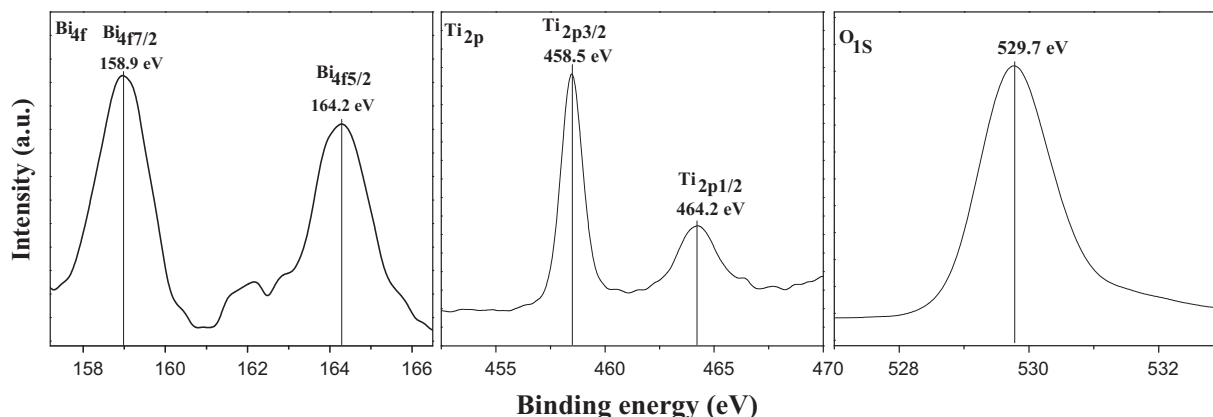
Fig. 3. XPS spectra of 1.0% Bi_2O_3/TiO_2 film.
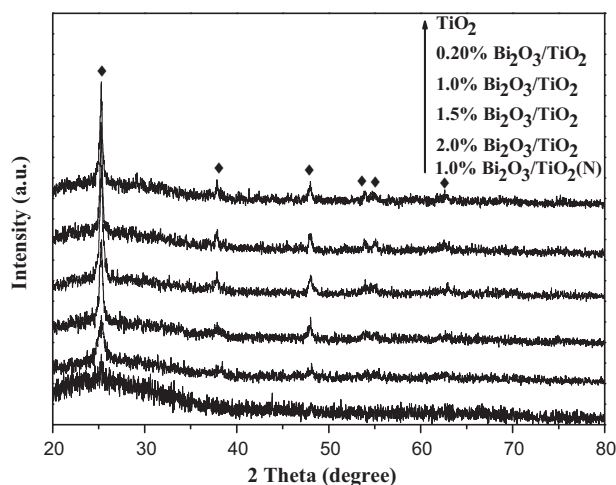
Fig. 4. XRD patterns of $X\%$ Bi_2O_3/TiO_2 and 1.0% $Bi_2O_3/TiO_2(N)$ films.
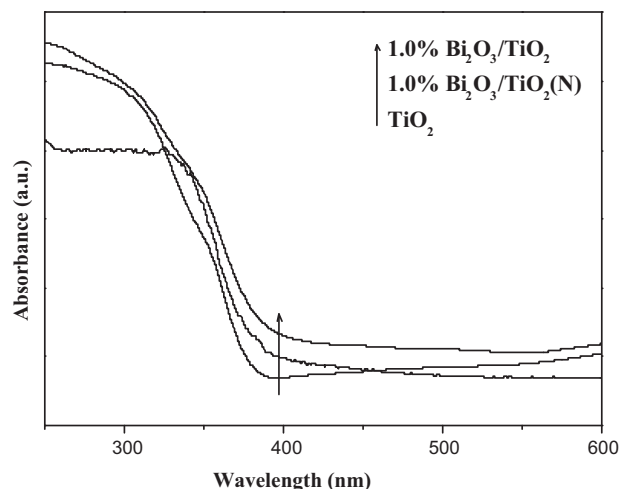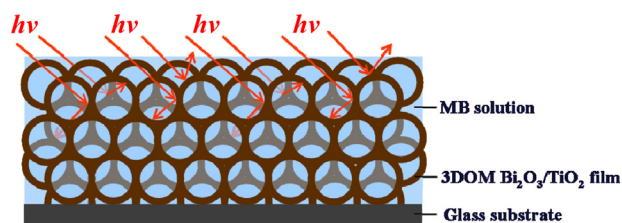

Fig. 5. UV–vis diffusion reflection spectra of different films.

Scheme 2. Illustration of the enhanced light harvest *via* multiple reflections in macropores of the Bi_2O_3/TiO_2 film.

film displayed only diffraction peaks characteristic of anatase TiO_2 (JCPDS 21-1272). No significant diffraction peaks indicative of Bi_2O_3 was observed even at Bi/Ti molar ratio of 2.0%, obviously due to the high dispersion of Bi_2O_3 nanoparticles with ultrasmall size. Meanwhile, no significant shift of the principal diffraction peaks corresponding to TiO_2 was found, which further confirmed that the Bi_2O_3 was present in a separate phase rather than incorporated into the TiO_2 lattice. With the increase of Bi_2O_3 content, the diffraction peaks turned broad, suggesting that the presence of Bi_2O_3 disturbed TiO_2 crystal growth. The board peak in $1.0\%Bi_2O_3/TiO_2(N)$ film could be mainly attributed to the thinner thickness comparing to that of $1.0\%Bi_2O_3/TiO_2$ film. The HRTEM image (Fig. S1) clearly showed cross between the (0 0 2) facet of β-Bi_2O_3 crystal with lattice distance of 0.31 nm [26] and the (1 0 1) facet of anatase TiO_2 crystal with lattice distance of 0.35 nm [27], leading to the formation of Bi_2O_3-TiO_2 heterojunctions.

The 1.0% Bi_2O_3/TiO_2 film displayed type IV N_2 adsorption–desorption isotherm with hysteresis loop indicative of mesoporous structure centered at 3.8 nm (Fig. S2). Since the 1.0% $Bi_2O_3/TiO_2(N)$ film showed the similar N_2 adsorption–desorption isotherm and pore size distribution curve to the 1.0% Bi_2O_3/TiO_2 film, we concluded that the mesoporous structure was formed *via* particle gathering during sol–gel process. Although the similar mesoporous structures, the 1.0% Bi_2O_3/TiO_2 film exhibited higher S_{BET} (43 m^2/g) than 1.0% $Bi_2O_3/TiO_2(N)$ film (31 m^2/g), obviously owing to the presence of ordered macropores. Additionally, 1.0% Bi_2O_3/TiO_2 film showed the highest S_{BET} comparing to other Bi_2O_3/TiO_2 films.

3.2. Optical property

As shown in Fig. 5, the UV–vis DRS spectra revealed that the pure anatase TiO_2 film displayed no spectral response in visible light area due to its big energy band gap (3.2 eV). As expected, the 1.0% Bi_2O_3/TiO_2 film exhibited strong absorbance for visible lights owing to photosensitization of Bi_2O_3 with narrow energy band gap (2.8 eV) [13]. The 1.0% Bi_2O_3/TiO_2 film exhibited stronger absorbance for both UV and visible lights than the 1.0% $Bi_2O_3/TiO_2(N)$ film, possibly owing to the enhanced light harvest *via* multiple reflections in macropores (see Scheme 2). Fig. 6 further demonstrated that the 1.0% Bi_2O_3/TiO_2 film exhibited stronger photocurrent density than the 1.0% $Bi_2O_3/TiO_2(N)$ film under visible light irradiation owing to the enhanced light harvest. Besides, the PL spectra (Fig. S3) revealed that the Bi_2O_3/TiO_2 film displayed weaker intensity of the peak around 427 nm than the pure TiO_2 film,

corresponding to the lower recombination rate between photoelectrons and holes [28]. This could be attributed to the formation of TiO_2-Bi_2O_3 heterojunctions which facilitated the electron transfer from Bi_2O_3 to TiO_2 [14,15] and thus reduced the photoelectron-hole recombination. With the increase of Bi_2O_3 content in Bi_2O_3/TiO_2 film up to Bi/Ti molar ratio of 1.0, the photoelectron-hole recombination rate decreased gradually owing to the enhanced number of heterojunctions. However, further increase in Bi content (Bi/Ti molar ratio > 1.0%) resulted in the enhanced photoelectron-hole recombination rate, possibly due to the agglomeration of Bi_2O_3 into big particles [12].
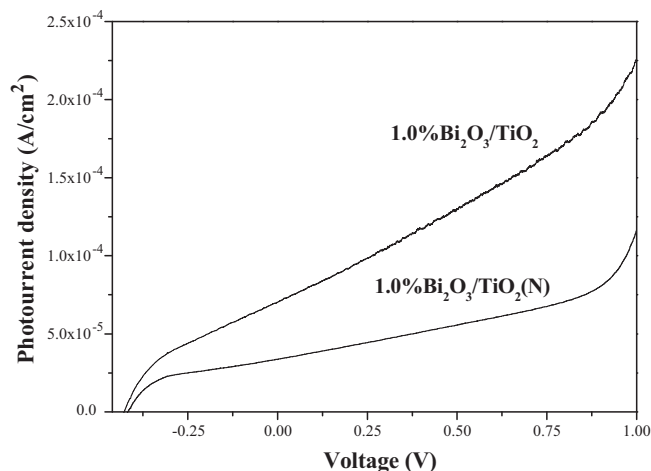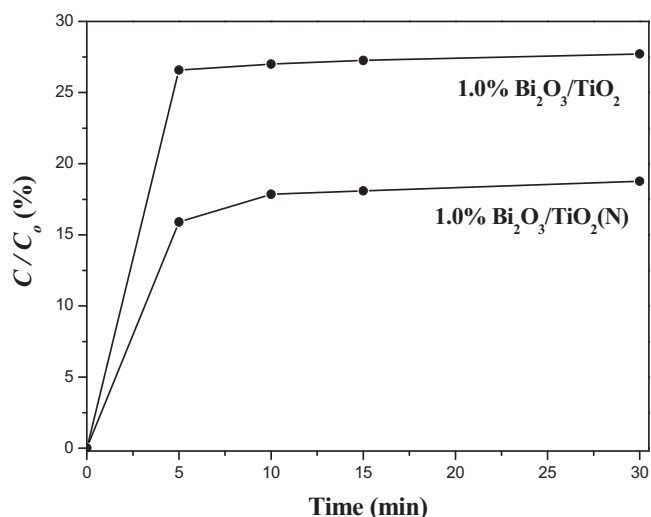

Fig. 6. Photocurrent response tests of 1.0% Bi_2O_3/TiO_2 and 1.0% $Bi_2O_3/TiO_2(N)$ films under visible light irradiation (300 W Xe lamp, $\lambda \geq 400$ nm).

Fig. 7. Adsorption process of MB on 1.0%Bi$_2$O$_3$/TiO$_2$ and 1.0%Bi$_2$O$_3$/TiO$_2$(N) films in aqueous solution. Test conditions: 5.0 mL 10 mg/L MB solution, three glass sheets coated with catalysts (2.0 cm × 2.5 cm), T = 30 °C.

3.3. Adsorption property

As shown in Fig. 7, 1.0% Bi$_2$O$_3$/TiO$_2$ film exhibited the higher saturated adsorption capacity for MB in aqueous solution than 1.0% Bi$_2$O$_3$/TiO$_2$(N) film, obviously owing to the larger S_{BET}. Meanwhile, it also displayed faster adsorption rate, which could be further confirmed by the UV–vis spectra (Fig. S4). Obviously, the ordered macropores facilitated the adsorption of MB molecules owing to the diminished diffusion limit. Meanwhile, it was interesting to see that 1.0% Bi$_2$O$_3$/TiO$_2$ film displayed stronger surface hydrophilicity than the 1.0% Bi$_2$O$_3$/TiO$_2$(N) film (see Fig. S5) possibly due to the cavity effect in micropores [21,29], which further promoted the adsorption of hydrophilic MB molecules.

### 3.4. Photocatalytic performances

The visible-light-driven photocatalytic degradation of MB in aqueous solution was employed as a probe to evaluate the activity of different film photocatalysts. Firstly, we examined the influence of the film thickness on the photocatalytic activity. The film thickness increased with the increasing content of PS microspheres deposited onto the glass surface, which was confirmed by both the calculation from Nagayama's theory [26] and the estimation from the FESEM images (Fig. S6). As shown in Fig. 8, the photocatalytic activity of 1.0% Bi$_2$O$_3$/TiO$_2$ film increased rapidly with the increase of thickness from 2.0 to 11 μm, which could be mainly attributed to the increased content of Bi$_2$O$_3$/TiO$_2$ photocatalyst in the reaction system. Moreover, the enhanced film thickness also promoted light harvest [27]. However, further increase in film thickness from 11 to 14 μm displayed very limited promoting effect on the activity, possibly due to the overlap of active sites which could not contact with the reactant molecules and/or be activated by lights [30]. In addition, very thick Bi$_2$O$_3$/TiO$_2$ film might damage the uniform distribution of Bi$_2$O$_3$/TiO$_2$ and even the ordered macroporous structure. Furthermore, the enhanced thickness might also reduce the film stability against leaching due to the decrease in the film-substrate interaction [31,32]. The optimum thickness of 1.0% Bi$_2$O$_3$/TiO$_2$ film was thus determined as 11 μm, which was obtained by using 0.20 wt% PS microspheres coated on the glass substrate.

As shown in Fig. 9, the pure anatase TiO$_2$ film exhibited very poor activity since it could not be activated by visible lights. The activity of the Bi$_2$O$_3$/TiO$_2$ film increased gradually with the increase
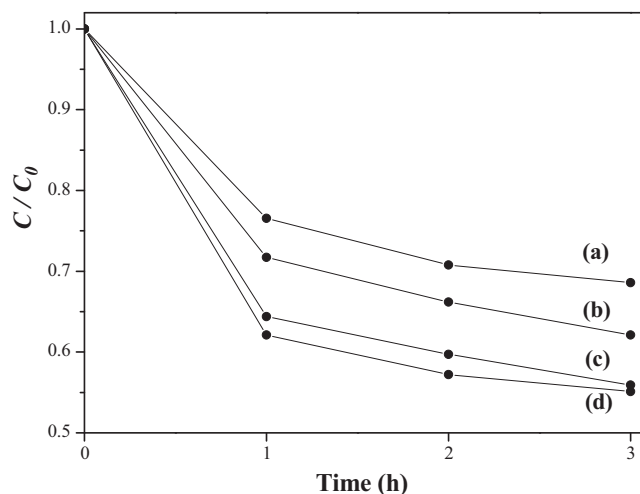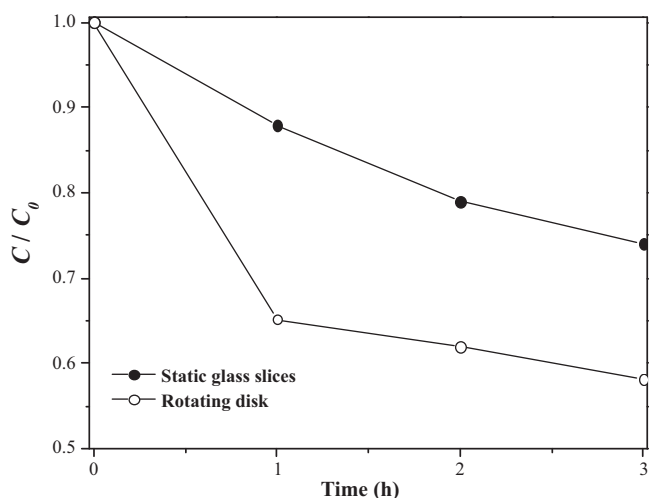

Fig. 8. Visible light driven photocatalytic degradation of MB on 1.0% Bi$_2$O$_3$/TiO$_2$ films prepared by using different contents (wt%) of PS microspheres: (a) 0.10, (b) 0.15, (c) 0.20 and (d) 0.30. Reaction conditions: 55 mL 10 mg/L MB aqueous solution, 6 glass slices (2.5 cm × 2.0 cm) coated by photocatalyst film, one 500 W Xe lamp ($\lambda \geq$ 420 nm), T = 30 °C, rotation speed of disk = 90 rpm.

of Bi$_2$O$_3$ content, which could be attributed to the enhanced photosensitizing effect and the reduced photoelectron-hole recombination rate due to the formation Bi$_2$O$_3$-TiO$_2$ heterojunctions. However, very high Bi$_2$O$_3$ content was harmful for the photocatalytic activity of the Bi$_2$O$_3$/TiO$_2$ film due to the gathering of Bi$_2$O$_3$ into big particles. The 1.0% Bi$_2$O$_3$/TiO$_2$ film was determined as the optimum photocatalyst. It exhibited much higher activity than 1.0% Bi$_2$O$_3$/TiO$_2$(N) film owing to the promoting effect of the ordered macropore structure, which facilitated the diffusion/adsorption of MB molecules and also enhanced light harvest *via* multiple reflections. Additionally, the combination effect of TiO$_2$ and Bi$_2$O$_3$ was also confirmed *via* comparing powder samples. From Fig. S7, it could be found that the Bi$_2$O$_3$ particle could harvest the visible light, and then efficiently extended the light absorption of TiO$_2$ to the visible light region. As a result, Fig. S8 presented the higher activity of 1.0%Bi$_2$O$_3$/TiO$_2$ than TiO$_2$, Bi$_2$O$_3$ and mixture of TiO$_2$ and Bi$_2$O$_3$ powders, obviously owing to the strong combination effect of Bi$_2$O$_3$ and TiO$_2$ *via* the formation Bi$_2$O$_3$-TiO$_2$ heterojunctions. Moreover,
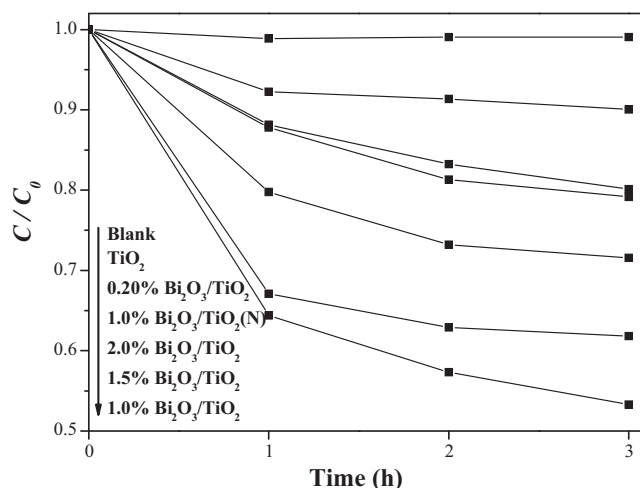
Fig. 9. Photocatalytic degradation of MB under visible light irradiation. Reaction conditions: 55 mL 10 mg/L MB aqueous solution, 6 glass slices (2.5 cm × 2.0 cm) coated by photocatalyst film, one 500 W Xe lamp ($\lambda \geq$ 420 nm), T = 30 °C, rotation speed of disk = 90 rpm.
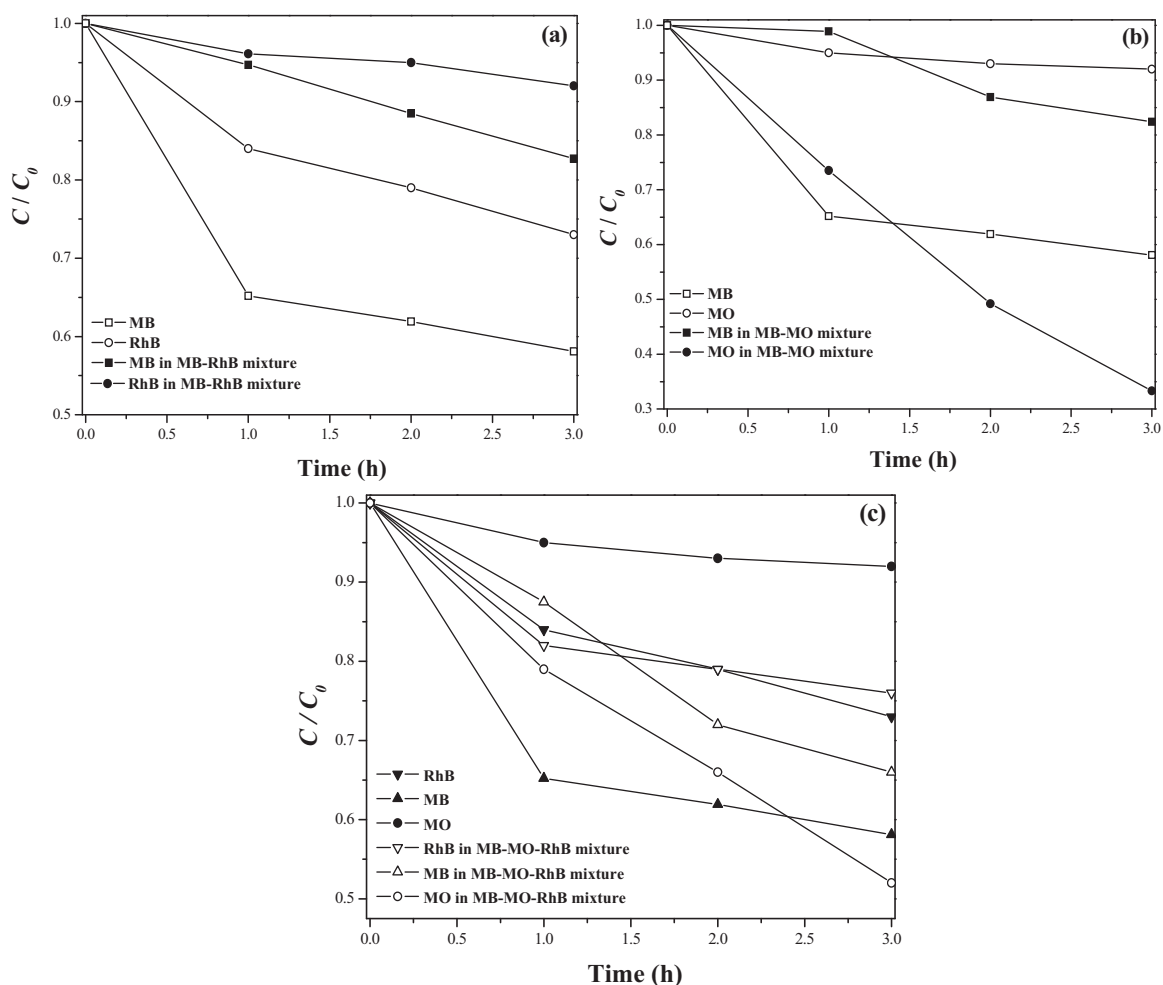
Fig. 10. Visible light driven photocatalytic degradation of MB on 1.0% Bi_2O_3/TiO_2 film coated on either the rotating disk or 6 static glass slices (2.5 cm × 2.0 cm) immersed in the solution. Reaction conditions are given in Fig. 9.

the obvious leaching of pure Bi_2O_3 particle after the reaction was demonstrated based on the ICP measurement.

Fig. 10 revealed that, during photocatalytic degradation of MB under visible light irradiation, 1.0% Bi_2O_3/TiO_2 film coated on the rotating disk exhibited much higher activity than that on the static glass slices with the same amount of Bi_2O_3/TiO_2. Obviously, 1.0% Bi_2O_3/TiO_2 film coated on the static glass slices immersed in MB solution could not effectively absorb light due to the shielding effect from the blue solution while 1.0% Bi_2O_3/TiO_2 film coated on the rotating disk could greatly reduce the shielding effect on light absorbance owing to the alternative exposure-immersion of the Bi_2O_3/TiO_2 film in the MB solution (see Fig. 1), leading to the enhanced photocatalytic activity.

Besides the MB degradation, the present reactor containing a rotating disk coated with 1.0% Bi_2O_3/TiO_2 film could also be used in visible-light-induced photocatalytic degradation of other organic dyes including RhB and MO (see the structural formula in Scheme S1) and reduction of Cr^{6+} in aqueous solution containing either single component or multiple components. The previous results demonstrated that their photocatalytic degradation followed different reactions mechanisms based on the intermediate chemicals determined by HPLC-MS analysis [33–35]. The RhB, MO and MB degradations were initiated *via* the de-ethylation route, the reduction of N=N double bond, and the ionization, followed by other oxidation steps involving ring-opening reaction. As shown in Fig. 11, during the photocatalytic degradation of mixed MB and RhB, both the MB and the RhB degradation yields decreased in comparison with those obtained using single MB or RhB since they consumed the same active sites including photo-generated holes and $^{\bullet}OH$ radicals resulted from oxidation of OH^- by holes [33]. However, during the photocatalytic degradation of mixed

Fig. 11. Visible-light-driven photocatalytic degradation of MB, RhB, MO in single-component solution and solutions containing mixed dyes in the reactor containing a rotating disk coated with the 1.0% Bi_2O_3/TiO_2 film under visible light irradiation. (a) MB-RhB, (b) MB-MO, and (c) MB-MO-RhB. Reaction conditions are given in Fig. 9.
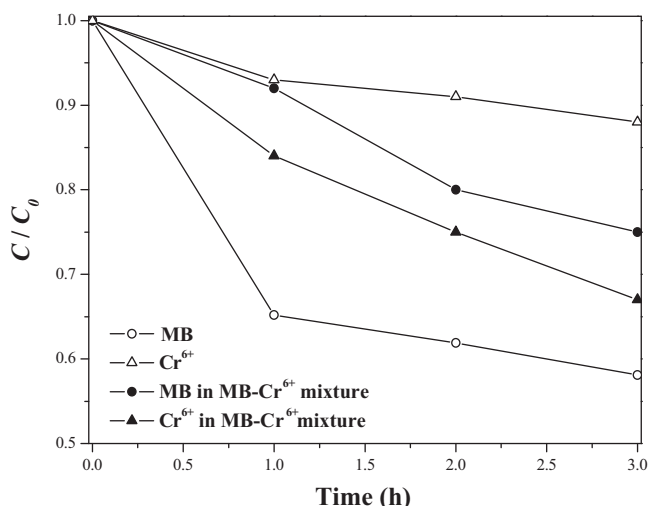
Fig. 12. Visible light driven photocatalytic degradation of MB, Cr^{6+} in single-component solution and MB-Cr^{6+} solution in the reactor containing a rotating disk coated with the 1.0% Bi_2O_3/TiO_2 film. Reaction conditions are given in Fig. 9.

MB and MO in aqueous solution, the degradation of MB was significantly suppressed while the degradation of MO was greatly promoted in comparison with those obtained using single MB or MO. This could be understood by considering the different reaction route. Since the MO molecular containing N=N double bond, its degradation was initiated by reduction route with direct consuming photoelectrons, followed by oxidation route with consuming photo-induced holes, while the MB followed oxidation route with consuming photo-induced holes [33]. Thus, the presence of MB promoted the degradation of MO since the degradation of MB consumed photo-induced holes and thus reduced their recombination with photoelectrons used for initiating MO degradation, leading to the enhanced MO degradation yield. The MB degradation yield decreased in the presence of MO since the subsequent degradation of MO also consumed photo-induced holes. Similar results were also observed in the photocatalytic degradation of mixed dyes (RhB, MB and MO). Furthermore, as shown in Fig. 12, the presence of MB greatly promoted photocatalytic reduction of Cr^{6+} since the photocatalytic degradation of MB consumed photo-induced holes and thus reduced their recombination with photoelectrons used for reducing Cr^{6+} to Cr^{3+}. However, the presence of Cr^{6+} was harmful for photocatalytic degradation of MB, possibly due to the strong adsorption of product Cr^{3+} ions on the photocatalyst surface [36], which might capture photo-induced holes used as key active sites for MB degradation.

4. Conclusion

In summary, we developed a facile approach to prepare ordered macroporous Bi_2O_3/TiO_2 film coated on the rotating disk, which exhibited high activity during liquid phase photocatalytic degradation of MB and mixed dyes or photocatalytic reduction of Cr^{6+} to Cr^{3+} under visible light irradiation. The Bi_2O_3-dopants showed photosensitizing effect on the TiO_2 toward spectral response in visible light area and also reduced photoelectron-hole recombination rate by forming Bi_2O_3-TiO_2 heterojunctions. Meanwhile, the ordered macropores favored the light-harvesting *via* multiple reflections, reactant adsorption owing to the diminished diffusion limit and the enhanced hydrophilicity. The rotating disk ensured the alternative exposure-immersion of the Bi_2O_3/TiO_2 film in the solution, which could efficiently reduced the shielding effect of the colorful solution for the light absorbance on the Bi_2O_3/TiO_2 film photocatalyst. This work supplied a powerful way for treating colorful wastewater by photocatalysis.

Appendix A. Supplementary data

Supplementary data associated with this article can be found, in the online version, at http://dx.doi.org/10.1016/j.apcatb.2013.11.040.

References

[1] M.R. Hoffmann, S.T. Martin, W.Y. Choi, D.W. Bahnemann, Chem. Rev. 95 (1995) 69–96.
[2] C.S. Guo, M. Ge, L. Liu, G.D. Gao, Y.C. Feng, Y.Q. Wang, Environ. Sci. Technol. 44 (2010) 419–425.
[3] X.B. Chen, S.M. Samuel, Chem. Rev. 107 (2007) 2891–2959.
[4] M.D. Hernández-Alonso, F. Fernando, S. Silvia, M.C. Juan, Energy Environ. Sci. 2 (2009) 1231–1257.
[5] J. Li, H.C. Zeng, J. Am. Chem. Soc. 129 (2007) 15839–15847.
[6] Y.N. Huo, X.L. Yang, J. Zhu, H.X. Li, Appl. Catal. B 106 (2011) 69–75.
[7] J. Zhu, J. Ren, Y.N. Huo, Z.F. Bian, H.X. Li, J. Phys. Chem. C 111 (2007) 18965–18969.
[8] N. Lakshminarasimhan, A.D. Bokare, W.Y. Choi, J. Phys. Chem. C 116 (2012) 17531–17539.
[9] Y.N. Huo, Z.F. Bian, X.Y. Zhang, Y. Jin, J. Zhu, H.X. Li, J. Phys. Chem. C 112 (2008) 6546–6550.
[10] H. Jia, H. Xu, Y. Hu, Y.W. Tang, L.Z. Zhang, Electrochem. Commun. 9 (2007) 354–360.
[11] W. Zhao, Y.F. Sun, N. Castellano, J. Am. Chem. Soc. 130 (2008) 2566–12567.
[12] Z.F. Bian, J. Zhu, S.H. Wang, Y. Cao, X.F. Qian, H.X. Li, J. Phys. Chem. C 112 (2008) 6258–6262.
[13] Y.Q. Wu, G.X. Lu, S.B. Li, J. Phys. Chem. C 113 (2009) 9950–9955.
[14] L.G. Wang, J.Y. Zhang, C.Z. Li, H.L. Zhu, W.W. Wang, T.M. Wang, J. Mater. Sci. Technol. 27 (2011) 59–63.
[15] Y. Bessekhouad, D. Robert, J.V. Weber, Catal. Today 101 (2005) 315–321.
[16] L.H. Lu, A. Eychmuller, Acc. Chem. Res. 41 (2008) 244–253.
[17] Z.F. Bian, J. Zhu, F.L. Cao, Y.N. Huo, Y.F. Lu, H.X. Li, Chem. Commun. 46 (2010) 8451–8453.
[18] K. Su, Z.H. Ai, L.Z. Zhang, J. Phys. Chem. C 116 (2012) 17118–17123.
[19] R. Daghrir, P. Drogui, D. Robert, Ind. Eng. Chem. Res. 52 (2013) 3581–3599.
[20] Y. Lu, H.T. Yu, S. Chen, X. Quan, H.M. Zhao, Environ. Sci. Technol. 46 (2012) 1724–1730.
[21] H. Xie, Y.Z. Li, S.F. Jin, J.J. Han, X.J. Zhao, J. Phys. Chem. C 114 (2010) 9706–9712.
[22] H. Chen, S. Chen, X. Quan, Y.B. Zhang, Environ. Sci. Technol. 44 (2010) 451–455.
[23] Y.L. Xu, Y. He, X.D. Cao, D.J. Zhong, J.P. Jia, Environ. Sci. Technol. 42 (2008) 2612–2617.
[24] J.X. Wang, Y.Q. Wen, X.J. Feng, Y.L. Song, L. Jiang, Macromol. Rapid Commun. 27 (2006) 188–192.
[25] J. Xu, Y.H. Ao, D.G. Fu, C.W. Yuan, Appl. Surf. Sci. 255 (2008) 2365–2369.
[26] Y.G. Ko, D.H. Shin, J. Phys. Chem. B 111 (2007) 1545–1551.
[27] A.K. Jena, P. Bhargava, Renew. Energy 53 (2013) 265–270.
[28] J.I.L. Chen, G.A. Ozin, J. Mater. Chem. 19 (2009) 2675–2678.
[29] M. Sadakane, T. Horiuchi, N. Kato, C. Takahashi, W. Ueda, Chem. Mater. 19 (2007) 5779–5785.
[30] S. Ito, S.M. Zakeeruddin, R. Humphry-Baker, P. Liska, R. Charvet, P. Comte, Adv. Mater. 18 (2006) 1202–1205.
[31] J. Shang, W. Li, Y.F. Zhu, J. Mol. Catal. A 202 (2003) 187–195.
[32] S. Ngamsinlapasathian, T. Sreethawong, Y. Suzuki, S. Yoshikawa, Sol. Energy Mater. Sol. Cells 86 (2005) 269–282.
[33] X. Li, J. Zhu, H.X. Li, Appl. Catal. B 123–124 (2012) 174–181.
[34] Y.C. Miao, G.F. Pan, Y.N. Huo, H.X. Li, Dyes Pigments 99 (2013) 382–389.
[35] H. Gnaser, M.R. Savina, W.F. Calaway, C.E. Trip, I.V. Veryovkin, M.J. Pellin, Int. J. Mass Spectrom. 245 (2005) 61–67.
[36] J.G. Wang, X.R. Li, X. Li, J. Zhu, H.X. Li, Nanoscale 5 (2013) 1876–1881.